Model Identification of a Small Omnidirectional Aquatic Surface Vehicle: a Practical Implementation

Keir Groves[1][2], Marin Dimitrov[2], Harriet Peel[2], Ognjen Marjanovic[2], Barry Lennox[2]

Abstract— This work presents a practical method of obtaining a dynamic system model for small omnidirectional aquatic vehicles. The models produced can be used to improve vehicle localisation, aid in the design or tuning of control systems and facilitate the development of simulated environments. The use of a dynamic model for onboard real-time velocity prediction is of particular importance for aquatic vehicles because, unlike ground vehicles, fast and direct measurement of velocity using encoders is not possible. Previous work on model identification of aquatic vehicles has focused on large vessels that are typically underactuated and have low controllability in the sway direction. In this paper it is demonstrated that the procedure for identifying the model coefficients can be performed quickly, without specialist equipment and using only onboard sensors. This is of key importance because the dynamic model coefficients will change with the payload. Two different thrust allocation schemes are tested, one of which is a known method and another is proposed here. Validation tests are performed and the models are shown to be suitable for their intended applications. Significant reduction in model error is demonstrated using the novel thrust allocation method that is designed to avoid deadbands in the thruster responses.

I. Introduction

A. Motivation

Although the field of autonomous surface vehicles (ASVs) is relatively well developed, the majority of the work to date has focused on large vehicles designed for operation in natural environments, such as seas or lakes.

Work on smaller ASVs that can be accurately controlled in confined environments is scarce, but there are very promising applications, including inspection and monitoring of nuclear storage pools or large industrial tanks. Due to the relative scale of a typical confined environment compared to a marine environment, localisation and control accuracy must be much higher; for example $\pm 1\,\mathrm{m}$ accuracy is usually considered to be sufficiently high in marine vehicles, while accuracy within $\pm 1\,\mathrm{cm}$ is often required in confined environments [1].

From a navigation perspective, the accuracy of localisation and control has a direct impact on the robot's ability to traverse narrow gaps and tight spaces whilst avoiding obstacles. This is of particular importance in nuclear applications where collisions may cause the robot and subsequently the surrounding area to become contaminated. Accurate control and localisation is also important with respect to the sensor package that is being deployed. For instance, radiation detectors are typically very sensitive to the distance from the object being measured and must be held still for a period of time while the measurement is taken.

This paper presents a mathematical model of a small overactuated ASV, MallARD (sMall Autonomous Robotic Duck) [2], and provides a method of determining model coefficients that is both fast and practical. The model developed has three principal uses:

1) To facilitate development in simulation. Specifically, the model is used onboard the El-MallARD hardware simulation [3], an omni-directional ground vehicle that, given a dynamic model, can mimic the physical behaviour of other robots, including aquatic platforms.

2) To improve the trajectory tracking control system by implementing a model-based tuning procedure (e.g internal model control) for the current PD controller or facilitating the development of more advanced model-based controllers, such as robust control or model predictive control.

3) To improve the robustness and precision of the location estimate by providing the SLAM algorithm with odometry information that is typically unavailable for small aquatic vehicles.

To expand upon the third point, the SLAM algorithm used presently is not fed odometry information and occasionally produces an incorrect match between scan data and the map, especially under aggressive manoeuvring. This causes the map to become corrupted and therefore invalidates the pose estimate. Because fast and direct measurement of velocity is infeasible for small vehicles in confined aquatic environments [5], the availability of a dynamic model that can give reliable velocity estimation is of marked importance.

However, one of the main practical challenges that hampers wide usage of system models is the unavailability of time-efficient identification of model parameters. This is particularly true in cases of vehicles that are designed to transport a variety of payloads, for which any change to the payload will change the hydrodynamic behaviour and therefore model coefficients. Hence, development of a simple method of identifying and updating model coefficients that does not require special facilities or equipment is particularly relevant in this area of application.

In preliminary work, the authors found that an obvious source of error in the model's prediction was the presence of deadbands in the thruster's responses during the transition between positive and negative thrust. Accordingly, a new thrust allocation, inspired by quadrotors, was developed and is tested thoroughly alongside the previous thrust allocation.

[1] keir.groves@manchester.ac.uk
[2] Department of Electrical and Electronic Engineering, University of Manchester, UK

B. Previous work

Dynamic models of aquatic vehicles have been identified for both surface [7], [8], [9], [10] and underwater vehicles [11], [6], [12]. However, the majority of the work on model identification of surface vehicles has been concerned with large marine ships (e.g., [13]). Smaller vehicles have been successfully modelled in [7], [8], which performed model identification on modified, rigid-hull, inflatable boats that were 4.5 m and 8.45 m long respectively. Also, the model of a smaller USV that was 1.5m long is provided in [9]. Although these vehicles are relatively small, they are all underactuated and therefore have limited controllability in the sway direction.

In [7], Sonnenburg and Woolsey provide a review of the system identification techniques that have been implemented on surface vehicles, ranging from black box neural network approaches to model-based approaches in both time and frequency domain. Some of the proposed approaches rely on open-loop experiments in order to obtain data used for model identification, whilst others collect data from closed-loop operation. In the work reported in this paper, all experiments were performed in open-loop to avoid the risk of control parameters having influence on model coefficients and a least squares method was used to derive the model coefficients.

C. Contribution

The main contributions of this paper are summarised as follows:

1) The development of a dynamic model structure that is suited to small omnidirectional surface vehicles;
2) A methodology for identifying model parameters that can be rapidly implemented without specialist equipment or facilities;
3) An alternate thrust allocation scheme that improves the accuracy of the dynamic model by avoiding the deadband in the thruster response.

II. The MallARD platform

The MallARD (Figure 1) is a holonomic aquatic surface vehicle that is designed for low-speed (0-1 m/s) inspection and monitoring tasks in confined environments. MallARD's mechanical design is comprised of two pontoons, two chassis plates and four thrusters with an overall footprint of 44×50 cm. Propulsion is provided by the thrusters, each of which is located at one of the four corners and angled at 45 degrees with respect to the forward direction. This layout ensures thrust and drag symmetry while allowing vectoring in the $X_b Y_b$ plane and rotation about the Z_b axis. On-board electronics comprise of a single-board computer, a microcontroller and four electronic speed controllers (ESCs) that receive PWM signals from the microcontroller and drive the thrusters. The on-board computer processes data from the SICK TIM 571 LiDAR and uses a SLAM algorithm (Hector mapping [14]) to calculate the vehicle's pose. MallARD can be operated with varying levels of autonomy, from joypad operation to autonomous waypoint navigation with a closed

loop trajectory tracking controller. A full description of the design is provided in [2].
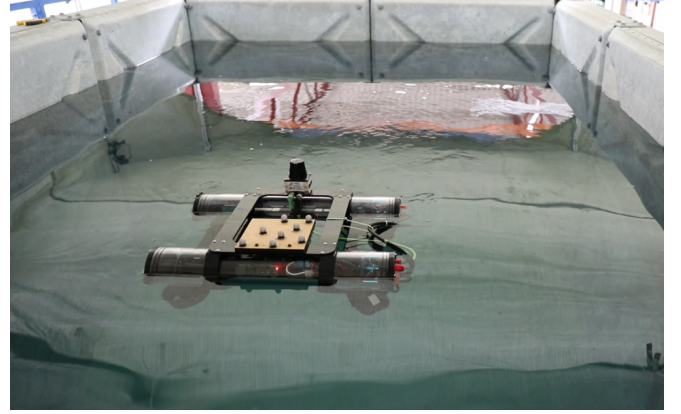

Fig. 1.   MallARD ASV operating in the test pool at the University of Manchester's robotics for extreme environments lab (REEL).

III. Three-DOF dynamic model and thrust allocation

MallARD is stable in roll and pitch and in a confined environment significant waves that would generate heave are not expected. Therefore, the full 6 degree of freedom (DOF) model can be simplified to a 3 DOF model to describe planar motion in terms of surge, sway and yaw [16].
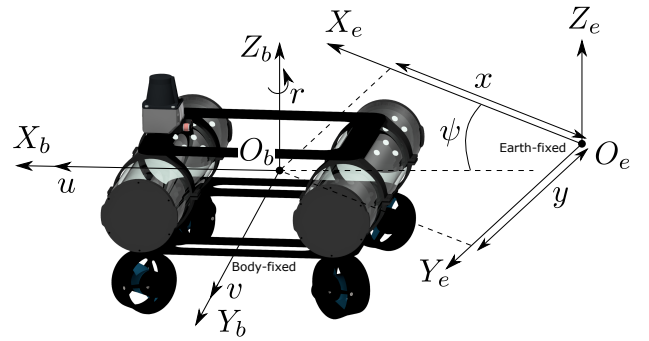
A. Reference frames and kinematics

Fig. 2. Schematic diagram showing the earth-fixed and body-fixed reference frames in relation to MallARD.

Figure 2 shows the two reference frames that are considered: the earth-fixed or inertial frame $O_e X_e Y_e$ and the moving body-fixed frame $O_b X_b Y_b$. Coordinate systems follow the conventions of [17] and the standard nomenclature of [15] and [10] is used throughout. The relationship between velocity in the earth-fixed frame and velocity in the body-fixed frame can be expressed as:

$$\dot{\boldsymbol{\eta}} = \boldsymbol{R}(\psi)\boldsymbol{\nu} \qquad (1)$$

where $\boldsymbol{\eta} = [x, y, \psi]^{\mathrm{T}}$, x and y are Cartesian positions in X_e and Y_e, ψ is the yaw angle in the earth-fixed frame, $\dot{\boldsymbol{\eta}} = \left[\dot{x}, \dot{y}, \dot{\psi}\right]^{\mathrm{T}}$ are the associated velocities in the

earth-fixed frame, $\boldsymbol{\nu} = [u, v, r]^{\mathrm{T}}$, u is the surge velocity, v is the sway velocity and r is the yaw rate in the body-fixed frame. The rotation matrix is given by:

$$\boldsymbol{R}\left(\psi\right) = \begin{bmatrix} \cos\psi & -\sin\psi & 0 \\ \sin\psi & \cos\psi & 0 \\ 0 & 0 & 1 \end{bmatrix} \qquad (2)$$

B. Dynamics

Following the methods of [10], [15], [6], [11], [9] and according to Newton's second law, the dynamic model of the MallARD in the body-fixed frame may be expressed by the following equations:

$$\boldsymbol{M}\dot{\boldsymbol{\nu}} + \boldsymbol{C}\left(\right)\boldsymbol{\nu} + \boldsymbol{D}\left(\boldsymbol{\nu}\right)\boldsymbol{\nu} = \boldsymbol{\tau} \qquad (3)$$

$$\boldsymbol{M} = \begin{bmatrix} m & 0 & 0 \\ 0 & m & 0 \\ -my_g & 0 & I_z \end{bmatrix} \qquad (4)$$

$$\boldsymbol{C}\left(\boldsymbol{\nu}\right) = \begin{bmatrix} 0 & 0 & -mv \\ 0 & 0 & mu \\ 0 & 0 & 0 \end{bmatrix} \qquad (5)$$

$$\boldsymbol{D}\left(\boldsymbol{\nu}\right) = \boldsymbol{D} + \boldsymbol{D}_N\left(\boldsymbol{\nu}\right) \qquad (6)$$

$$\boldsymbol{D} = -\begin{bmatrix} X_u & 0 & 0 \\ 0 & Y_v & 0 \\ 0 & 0 & N_r \end{bmatrix} \qquad (7)$$

$$\boldsymbol{D}_N\left(\boldsymbol{\nu}\right) = \begin{bmatrix} -X_{|u|u}\left|u\right| & 0 & 0 \\ 0 & -Y_{|v|v}\left|v\right| & 0 \\ -N_{|u|u}\left|u\right| & 0 & -N_{|r|r}\left|r\right| \end{bmatrix} \qquad (8)$$

$$\boldsymbol{\tau} = \begin{bmatrix} \tau_u \\ \tau_v \\ \tau_r \end{bmatrix} = \begin{bmatrix} X_F F_u \\ Y_F F_v \\ N_F F_r \end{bmatrix} \qquad (9)$$

where $\boldsymbol{M}\dot{\boldsymbol{\nu}}$ is the vector of inertial forces, $\boldsymbol{C}\left(\boldsymbol{\nu}\right)\boldsymbol{\nu}$ is the vector of centripetal forces, $\boldsymbol{D}\left(\boldsymbol{\nu}\right)\boldsymbol{\nu}$ is the vector of drag forces, $\boldsymbol{\tau}$ is the vector of propulsion forces and moments, m is the vehicle mass, I_z is the rotational inertia about the Z_b axis, y_g is the coordinate of the centre of gravity in the Y_b axis, X_u, Y_v, N_r, are the linear drag coefficients and $X_{|u|u}$, $Y_{|v|v}$, $N_{|r|r}$, $N_{|u|u}$ are the nonlinear drag coefficients, F_u, F_v, F_r are the control signals from the joypad or trajectory tracking controller and X_F, Y_F, N_F are the linear force coefficients.

It should be noted that added mass terms have been omitted to reduce the number of coefficients being identified and avoid over parametrisation. However, the dominant effects of added masses are accounted for by the inclusion of the corresponding coefficients in the identified system model.

The choice of terms used in the model described in Equations 3-9 was based on observations of the dynamic response of MallARD and consistency as well as significance of model parameter values estimated across repeated datasets. When MallARD is driven and allowed to drift in the X_b axis, repeatable patterns of yaw motion about the Z_b axis are induced, this indicates coupling between motion in the X_b axis and rotation about the Z_b axis. Such coupling is somewhat
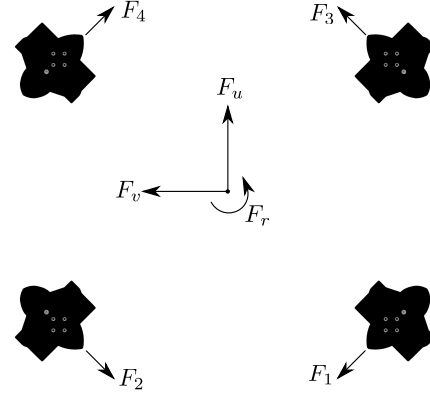

Fig. 3. Schematic diagram of MallARD's thruster layout. F_1-F_4 are forces applied on MallARD by the thrusters.

expected since MallARD is least symmetrical about the X_b axis due to the presence of cables connecting its pontoons. Alongside the coupled terms present in Equations 3-9, linear coupled drag terms, coupled force terms and nonlinear force functions were also initially included in the model. However, identified coefficients were either near zero or not repeatable across datasets and therefore were excluded from the model.

C. Thrust allocation

Figure 3 shows the thruster layout present on the MallARD. In the present work, two different thrust allocation schemes are used. The first is a standard method used previously by the authors in [2], termed here as the MP (Moore–Penrose) allocation. For this allocation, individual thruster commands $\begin{bmatrix} F_1 & F_2 & F_3 & F_4 \end{bmatrix}^{\mathrm{T}}$ are calculated by multiplying the vector of joypad commands $\begin{bmatrix} F_u & F_v & F_r \end{bmatrix}^{\mathrm{T}}$ by the inverted thrust allocation matrix $\boldsymbol{T}^\dagger$:

$$\begin{bmatrix} F_1 & F_2 & F_3 & F_4 \end{bmatrix}^{\mathrm{T}} = \boldsymbol{T}^\dagger \begin{bmatrix} F_u & F_v & F_r \end{bmatrix}^{\mathrm{T}} \qquad (10)$$

where $\boldsymbol{T}^\dagger$ is the Moore-Penrose inverse of $\boldsymbol{T}$, which is defined in [2] for MallARD.

The second thrust allocation scheme, termed the AF (always forward) allocation, was proposed here to overcome issues associated with the deadband. In the AF method, all of the thrusters are continuously operating and providing a positive force in their respective frames. With all thrusters operating at the same level, slightly above the deadband, the resultant thrust in the body frame will be zero, due to the symmetry of the thruster layout in the X_b and Y_b axes. To generate thrust in a given direction in the body frame, the input to two particular thrusters is increased equally; for example, to produce forward motion in X_b, the inputs to thrusters F_3 and F_4 are increased. The thruster command values never drop below a positive threshold F_{os} that prevents them from entering the deadband. Table I presents the algorithm used to generate the individual thruster command signals F_1-F_4 from the joypad inputs.

TABLE I

Input	F'_1	F'_2	F'_3	F'_4
if $F_u > 0$	0	0	$|F_u|$	$|F_u|$
if $F_u < 0$	$|F_u|$	$|F_u|$	0	0
else	0	0	0	0
if $F_v > 0$	$|F_v|$	0	$|F_v|$	0
if $F_v < 0$	0	$|F_v|$	0	$|F_v|$
else	0	0	0	0
if $F_r > 0$	$|F_r|$	0	0	$|F_r|$
if $F_r < 0$	0	$|F_r|$	$|F_r|$	0
else	0	0	0	0
	F_{os}	F_{os}	F_{os}	F_{os}

$$F_k = \sum F'_k \tag{11}$$

IV. EXPERIMENTS AND MODEL IDENTIFICATION

A. Data collection

For each of the two thrust allocations, namely MP and AF, a total of seven sets of data were collected, referred to as $S1$-$S7$ with an optional ending of $-MP$ or $-AF$ where it is necessary to distinguish between data collected using the two thrust allocations. The first three sets ($S1$-$S3$) were used for model identification. When generating each of these sets, excitation was limited to a single DOF as much as was practicable while avoiding boundaries of the confined area, i.e. the pool walls. For the first dataset ($S1$) MallARD was dominantly excited by F_u, for the second set ($S2$) by F_v and for the third set ($S3$) by F_r. The excitation signals F_u, F_v, F_r for each of the three sets were generated using the joypad, as a series of pulses in the positive and negative directions with varying amplitudes and lengths. It was not possible to use predetermined excitation signals due to the limited pool size (2.4×3.6 m Figure 1), which is a typical constraint and a limitation of conducting experiments under open-loop conditions. Throughout the experiments MallARD was kept at least 0.5 m from the pool walls, and for consistency the same person operated the joypad. Datasets four to six ($S4$-$S6$) were used for the first stage of validation and were collected from a repeat of the experiments performed to obtain datasets $S1$-$S3$. Dataset seven ($S7$) is the final validation set, for which MallARD was driven around the pool with excitation combined across the three degrees of freedom. Dataset $S7$ contains a variety of typical motion patterns, including figures of eight, circles and squares.

For each dataset, Mallard's pose in the earth-fixed frame (from LiDAR based SLAM) and the joypad inputs were recorded. The respective rates for the SLAM's pose output and joypad were 15 Hz and 100 Hz.

B. Model identification

To perform model identification, Equations 3-9 are multiplied out and coefficients are grouped as follows:

$$\dot{u} = vr + \left(X_{|u|uc}\,|u| + X_{uc}\right)u + X_{Fc}F_u$$
$$\dot{v} = -ur + \left(Y_{|v|vc}\,|v| + Y_{vc}\right)v + Y_{Fc}F_v \tag{12}$$
$$\dot{r} = N_{udc}\dot{u} + \left(N_{|r|rc}\,|r| + N_{rc}\right)r + N_{|u|uc}\,|u|\,u + N_{Fc}F_r$$

where $X_{|u|uc} = \frac{X_{|u|u}}{m}$, $X_{uc} = \frac{X_u}{m}$, $X_{Fc} = \frac{X_F}{m}$, $Y_{|v|vc} = \frac{Y_{|v|v}}{m}$, $Y_{vc} = \frac{Y_v}{m}$, $Y_{Fc} = \frac{Y_F}{m}$, $N_{udc} = \frac{my_g}{I_z}$, $N_{|r|rc} = \frac{N_{|r|r}}{I_z}$, $N_{rc} = \frac{N_r}{I_z}$, $N_{|u|uc} = \frac{N_{|u|u}}{I_z}$, $N_{Fc} = \frac{N_F}{I_z}$.

The model given in Equation 12 is then discretised and arranged into the form $\boldsymbol{a} = \boldsymbol{B}\boldsymbol{\theta}$ such that coefficients may be determined using the least squares method:

$$\boldsymbol{\theta}^* = \boldsymbol{B} \backslash \boldsymbol{a} \tag{13}$$

where $\backslash$ is the MATLAB backslash operator, $\boldsymbol{a}$ is the column vector of output measurements, $\boldsymbol{\theta}$ is the row vector of coefficients, $\boldsymbol{\theta}^*$ is the vector of estimated model coefficients and $\boldsymbol{B} = \begin{bmatrix} \boldsymbol{b}_1^{\mathrm{T}} & \dots & \boldsymbol{b}_N^{\mathrm{T}} \end{bmatrix}^{\mathrm{T}}$ is the regressor matrix of measured data that is independent of the coefficients.

Using measurements from datasets $S1$-$S3$, the model coefficients are determined in four steps. First the uncoupled coefficients are estimated for each DOF. To determine coefficients $X_{|u|uc}$, X_{uc} and X_{Fc}, dataset $S1$ was used and the variables of Equation 13 are given as:

$$a_k = \frac{u_k - u_{k-1}}{\Delta t} - v_{k-1}r_{k-1}$$
$$\boldsymbol{b_k} = \begin{bmatrix} |u_{k-1}|\,u_{k-1} & u_{k-1} & F_{u\,k-1} \end{bmatrix} \tag{14}$$
$$\boldsymbol{\theta} = \begin{bmatrix} X_{|u|uc} & X_{uc} & X_{Fc} \end{bmatrix}$$

To determine coefficients $Y_{|v|vc}$, Y_{vc} and Y_{Fc} dataset $S2$ was used and the variables of Equation 13 are:

$$a_k = \frac{v_k - v_{k-1}}{\Delta t} + u_{k-1}r_{k-1}$$
$$\boldsymbol{b_k} = \begin{bmatrix} |v_{k-1}|\,v_{k-1} & v_{k-1} & F_{v\,k-1} \end{bmatrix} \tag{15}$$
$$\boldsymbol{\theta} = \begin{bmatrix} Y_{|v|vc} & Y_{vc} & Y_{Fc} \end{bmatrix}$$

To determine coefficients $N_{|r|rc}$, N_{rc} and N_{Fc} dataset $S3$ was used and the variables of Equation 13 are:

$$a_k = \frac{r_k - r_{k-1}}{\Delta t}$$
$$\boldsymbol{b_k} = \begin{bmatrix} |r_{k-1}|\,r_{k-1} & r_{k-1} & F_{r\,k-1} \end{bmatrix} \tag{16}$$
$$\boldsymbol{\theta} = \begin{bmatrix} N_{|r|rc} & N_{rc} & N_{Fc} \end{bmatrix}$$

Notice that the coupled terms are not included in Equations 16. This is because coupled coefficients N_{udc} and $N_{|u|uc}$ cannot be identified using this dataset since there is minimal movement and no excitation in the X_b axis. To address this, dataset $S1$ was used once more and the previously determined coefficients $X_{|u|uc}$, X_{uc} and X_{Fc} were used to form $\boldsymbol{a}$:

$$a_k = \frac{r_k - r_{k-1}}{\Delta t} - \left(N_{|r|rc}\,|r_{k-1}| + N_{rc}\right)r_{k-1}$$
$$\quad - N_{Fc}\,r_{Fk-1}$$
$$\boldsymbol{b_k} = \begin{bmatrix} |u_{k-1}|\,u_{k-1} & \frac{u_{k-1}-u_{k-2}}{dt} \end{bmatrix} \tag{17}$$
$$\boldsymbol{\theta} = \begin{bmatrix} N_{|u|uc} & N_{udc} \end{bmatrix}$$

Coeff.	MP allocation	AF allocation
X_{uc}	-0.10	-0.20
$X_{\|u\|uc}$	-1.67	-1.74
X_{Fc}	0.15	0.14
Y_{vc}	-0.23	-0.23
$Y_{\|v\|vc}$	-1.26	-0.80
Y_{Fc}	0.26	0.20
N_{rc}	-0.73	-0.48
$N_{\|r\|rc}$	-0.30	-0.20
N_{Fc}	1.39	1.3
N_{udc}	-0.14	0.04
$N_{\|u\|uc}$	1.07	0.63

Fig. 4. Plot (a) shows measured velocity v versus 15 step ahead model prediction for the $S5$-MP dataset and Plot (b) displays the dominant excitation F_v.

Excitation axis	Dataset	RMS error MP allocation	RMS error AF allocation
X_b	$S4$	2.3 cm/s	1.8 cm/s
Y_b	$S5$	3.5 cm/s	2.2 cm/s
Z_b	$S6$	0.10 rad/s	0.07 rad/s

To identify model parameters, pose information in the earth-fixed frame is converted to velocity using the five-point stencil method. Earth-fixed velocity is then converted to body-fixed velocity using Equation 1.

Table II lists the coefficients obtained for both the MP and AF thrust allocations.

V. RESULTS AND DISCUSSION

The two developed models (MP and AF) are compared using validation data sets ($S4$-$S7$). All results presented in this section are based on a 15 step (one second) ahead velocity prediction. This horizon length was selected as it was deemed to be appropriate for model-based control and providing additional information to improve SLAM estimates.

Velocity predictions at time i are generated by taking the velocity measurement at time $i - 15$ and recursively evaluating the system model, given in Equation 12, for 15 subsequent time steps. Joypad inputs F_u, F_v, F_r were resampled at 15 Hz to time align them with velocity measurements. Error vectors are obtained by subtracting predicted from measured velocity values.

A. Results for single-axis excitation

Datasets $S4$-$S6$ were used to generate velocity predictions with excitation limited to a single axis as much as possible while avoiding collisions with walls. Figure 4 shows an example of a measured versus predicted velocity plot using dataset $S5$-MP. Under dominant excitation in the Y_b axis, predicted velocity tracks measured velocity well and similar results were obtained by evaluating the developed models on the other five associated datasets. For brevity their plots are omitted and the derived RMS error values are presented in Table III. Although all errors shown in Table III are generally low, the AF allocation consistently outperforms the MP allocation.

B. Results for multi-axis excitation

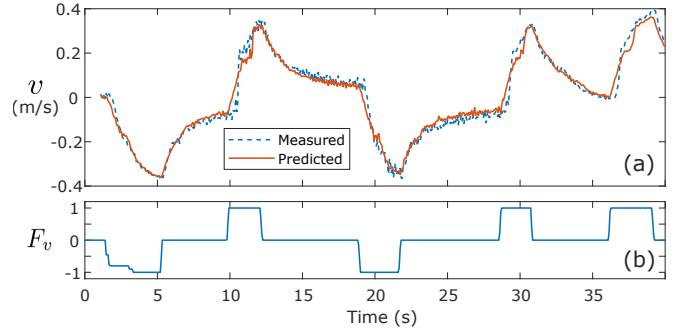To test motion prediction under combined excitation in F_u, F_v and F_r, the final dataset $S7$ was employed. Figure 5 displays a sample of the measured and predicted velocities in the X_b, Y_b and Z_b axes alongside the corresponding histograms for the MP thrust allocation, while Figure 6 displays the same plots for the AF thrust allocation. These plots clearly demonstrate the benefits of using the AF over the MP thrust allocation: RMS errors are approximately halved and the histograms are more Gaussian in shape. Figure 7 displays a sample autocorrelation of prediction errors for the Y_b axis. Results clearly indicate that the prediction errors corresponding to AP allocation are much closer to white, as indicated by significantly smaller autocorrelation components for non-zero lag. Similar results are obtained for the remaining two axes but are omitted here for brevity. Better performance of the AF thrust allocation under combined excitation was expected, as the deadband present in the MP allocation has a greater impact on the axis in which thrust is first applied; if thrust is added onto a second axis, the deadband has already been overcome and the thrust response changes, causing prediction error.

VI. CONCLUSIONS

Developed dynamic models of an aquatic surface vehicle were extensively evaluated and found to be sufficiently accurate in terms of the test metric, which is one second ahead velocity prediction. The accurate and reliable performance of the models in validation tests using this metric confirms their suitability for model-based control applications as well as the provision of improvements in the accuracy and precision of pose estimation. The dynamic models developed are already being used by the authors for software development in full-system simulations.

Although both thrust allocations produced dynamic models with low error, the new AF thrust allocation showed
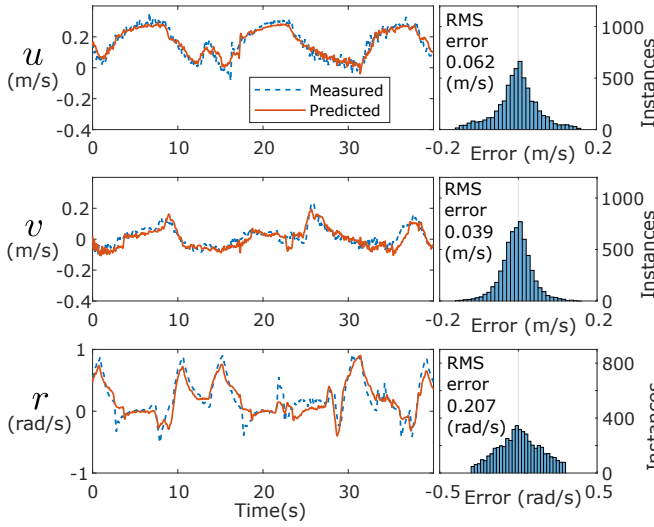
Fig. 5. Plots showing a 40 s sample of measured velocities against their 15 step ahead predictions for the three axes. Alongside each velocity plot is the associated error histogram and RMS error value, both derived from prediction error over 400 s. Excitation was applied to all three axes and the MP thrust allocation was used.
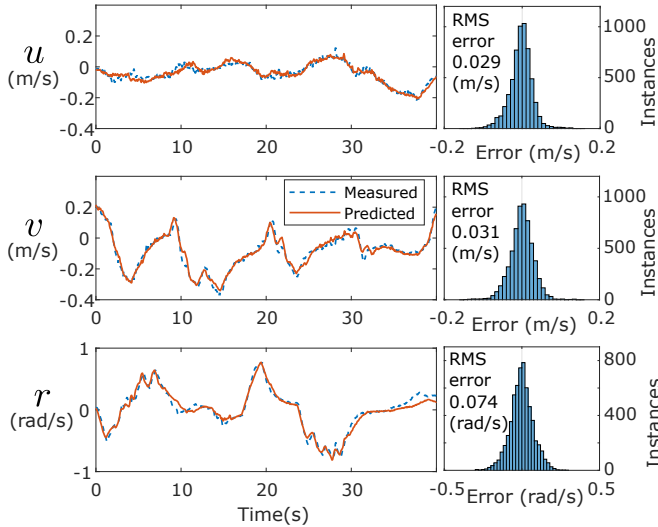

Fig. 6. Plots showing the same information as presented in Figure 5 but generated using the AF thrust allocation data.

significant improvement, especially for the angular velocity prediction.

Fig. 7. Normalised Autocorrelations for velocity prediction error in the Y_b axes, constructed using the $S7$ dataset

REFERENCES

[1] D. A. Duecker, A. R. Geist, M. Hengeler, E. Kreuzer, M.A. Pick, V. Rausch, E. Solowjow, "Embedded spherical localization for micro underwater vehicles based on attenuation of electro-magnetic carrier signals", Sensors, Vol. 17 no. 5, pp. 959, 2017.

[2] K. Groves, A. West, K. Gornicki, S. Watson, J. Carrasco, B. Lennox, MallARD: "An autonomous aquatic surface vehicle for inspection and monitoring of wet nuclear storage facilities", Robotics Vol. 8, no. 2, pp. 47, 2019.
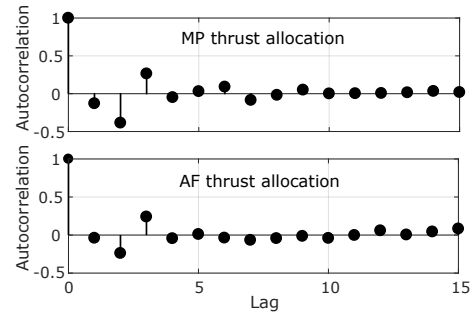
[3] C. Lennox, K. Groves, V. Hondru, F. Arvin, K. Gornicki, B. Lennox, "Embodiment of an aquatic surface vehicle in an omnidirectional ground robot", in: 2019 IEEE International Conference on Mechatronics (ICM), March, 2019, pp. 182–186.

[4] A. Mallios, "Sonar scan matching for simultaneous localization and mapping in confined underwater environments", Ph.D. thesis, University of Girona, 2014.

[5] J. Monroy-Anieva, C. Rouviere, E. Campos-Mercado, T. Salgado-Jimenez, L. Garcia-Valdovinos, "Modeling and Control of a Micro AUV: Objects Follower Approach", Sensors Vol. 18 no. 8, pp. 2574, 2018

[6] O. Hegrenaes, O. Hallingstad, "Model-aided INS with Sea Current Estimation for Robust Underwater Navigation", IEEE Journal of Oceanic Engineering Vol. 36, no. 2, pp. 316–337, 2011.

[7] C. R. Sonnenburg, C. A. Woolsey, "Modeling, identification, and control of an unmanned surface vehicle", Journal of Field Robotics Vol. 30, no. 3, pp. 371–398, 2013.

[8] B. Eriksen, M. Breivik, "Modeling, Identification and Control of High-Speed ASVs: Theory and Experiments", Sensing and Control for Autonomous Vehicles: Applications to Land, Water and Air Vehicles, Springer International Publishing, 2017, pp. 407–431.

[9] C. Li, J. Jiang, F. Duan, W. Liu, X. Wang, L. Bu, Z. Sun, G. Yang, "Modeling and experimental testing of an unmanned surface vehicle with rudderless double thrusters", Sensors Vol. 19 no. 9, pp. 2051, 2019.

[10] R. Skjetne, O. N. Smogeli, T. I. Fossen, "A nonlinear ship manoeuvering model: Identification and adaptive control with experiments for a model ship", Modelling, Identification and Control, Vol. 25 no. 1, pp. 3–27, 2004.

[11] S. Arnold, L. Medagoda, "Robust model-aided inertial localization for autonomous underwater vehicles", in: IEEE International Conference on Robotics and Automation (ICRA), Brisbane, Australia, May 2018, pp. 1–9.

[12] A. Alessandri, M. Caccia, G. Indiveri, G. Veruggio, "Application of LS and EKF techniques to the identification of underwater vehicles", in: Proceedings of the 1998 IEEE International Conference on Control Applications, Trieste, Italy, Sep. 1998, pp. 1084–1088.

[13] C. G. Källström, K. J. Åström, "Experiences of system identification applied to ship steering", Automatica Vol. 17, no. 1, pp. 187–198, 1981.

[14] S. Kohlbrecher, J. Meyer, O. von Stryk, U. Klingauf, "A flexible and scalable SLAM system with full 3D motion estimation", in: Proc. IEEE International Symposium on Safety, Security and Rescue Robotics (SSRR), Koyoto, Japan, Dec. 2011.

[15] T. I. Fossen, Guidance and control of ocean vehicles, Wiley New York, 1994.

[16] D. Mu, G. Wang, Y. Fan, X. Sun, B. Qiu,"Modeling and Identification for Vector Propulsion of an Unmanned Surface Vehicle: Three Degrees of Freedom Model and Response model", Sensors Vol. 18, no. 6, pp. 1889, 2018.

[17] T. Foote, M. Purvis, Rep 103 standard units of measure and coordinate conventions, Tech. Rep., Open Robotics, 2014. [Online]. Available: http://www.ros.org/reps/rep-0103.html, Date last accessed: Sep. 2019.

[18] P. Merriaux, Y. Dupuis, R. Boutteau, P. Vasseur, X. Savatier, "A Study of Vicon System Positioning Performance", Sensors Vol. 17, no. 7, pp. 1591, 2017.